subsequently eroded the layer, reducing peak concentration by 50% after 30 hours. Consideration of a local reduction in eddy diffusivity, typically encountered at the pycnocline, further increases layer intensity and duration. Importantly, we predict layer formation for shear rates ($S = 0.12\ s^{-1}$) comparable to those observed in thin layers (up to $S = 0.088\ s^{-1}$) (*1*, *4*), particularly considering that the latter likely underestimate peaks in shear because of coarse (meter-scale) sampling (*1*, *4*). Furthermore, recent high-resolution measurements find S in excess of $0.5\ s^{-1}$ in coastal waters (*26*), although the temporal coherence of these events remains to be determined.

Given the wide range of environmental conditions and species associated with thin layers, it is unlikely that a single mechanism is responsible for all layers (*27*). Although several mechanisms have been hypothesized, including in situ growth (*24*), buoyancy (*27*), and motility toward optimal resource levels (*5*), straining of a phytoplankton patch by shear is currently the most invoked (*4*, *16*, *24*, *27*). Our findings offer an alternative explanation of the role of shear: Regions of enhanced shear disrupt vertical motility and trigger sharp-peaked cell accumulations *ex novo* (Fig. 5B). This could occur routinely in natural water bodies because many species of phytoplankton are gyrotactic (*28*). Contrary to straining, gyrotactic trapping predicts that a mixture of phytoplankton species with differing gyrotactic behavior (e.g., B) will be sorted into multiple monospecific layers at different depths: Such vertical species separation is often observed in the ocean (*29*) and can affect zooplankton foraging and the spread of viral epidemics.

Gyrotactic trapping suggests that stabilization against tumbling might represent an evolutionarily selected trait for vertically migrating phytoplankton species. The parameter B^{-1} measures a cell's stability against overturning by shear. Whereas no stabilization ($B^{-1} = 0$) leaves the cell at the mercy of flow even at very small shear rates, stabilization is limited by biomechanical constraints (e.g., how bottom-heavy a cell can be) and excessive stabilization hinders maneuverability in exploiting nutrient patches and escaping predators. Although a simple model suggests that biomechanical constraints are not the only determinants of cell stability (*23*), further investigation is needed to establish the importance of stabilization in determining cell morphology.

The importance of motility in governing the spatial distribution of microorganisms in the ocean has been emphasized in recent years, chiefly for bacteria navigating patchy distributions of organic matter (*30*, *31*). Here we have demonstrated that motility and shear can generate intense thin layer accumulations of phytoplankton by gyrotactic trapping. By focusing resources, thin layers shape ecological interactions and can significantly affect trophic transfer and biogeochemical fluxes (*7*). Our results reveal how prominent macroscopic features of the marine landscape can originate from the microscopic coupling between flow and the motility of some of its smallest inhabitants.

References and Notes

1. M. M. Dekshenieks *et al*., *Mar. Ecol. Prog. Ser.* **223**, 61 (2001).
2. T. G. Nielsen, T. Kiørboe, P. K. Bjørnsen, *Mar. Ecol. Prog. Ser.* **62**, 21 (1990).
3. D. W. Townsend, N. R. Pettigrew, A. C. Thomas, *Deep-Sea Res. Part II Top. Stud. Oceanogr.* **52**, 2603 (2005).
4. J. P. Ryan, M. A. McManus, J. D. Paduan, F. P. Chavez, *Mar. Ecol. Prog. Ser.* **354**, 21 (2008).
5. P. K. Bjørnsen, T. G. Nielsen, *Mar. Ecol. Prog. Ser.* **73**, 263 (1991).
6. M. A. McManus *et al*., *Mar. Ecol. Prog. Ser.* **261**, 1 (2003).
7. T. J. Cowles, R. A. Desiderio, M. Carr, *Oceanography* **11**, 4 (1998).
8. A. L. Alldredge *et al*., *Mar. Ecol. Prog. Ser.* **233**, 1 (2002).
9. R. Lasker, *Fish. Bull. (Washington)* **73**, 453 (1975).
10. P. L. Donaghay, T. R. Osborn, *Limnol. Oceanogr.* **42**, 1283 (1997).
11. S. Yamochi, T. Abe, *Mar. Biol. (Berl.)* **83**, 255 (1984).
12. J. O. Kessler, *Nature* **313**, 218 (1985).
13. A. Genin, J. S. Jaffe, R. Reef, C. Richter, P. J. S. Franks, *Science* **308**, 860 (2005).
14. J. Hill, O. Kalkanci, J. L. McMurray, H. Koser, *Phys. Rev. Lett.* **98**, 068101 (2007).
15. F. P. Bretherton, L. Rothchild, *Proc. R. Soc. London Ser. B* **153**, 490 (1961).
16. P. J. S. Franks, *Deep-Sea Res. Part I Oceanogr. Res. Pap.* **42**, 75 (1995).
17. T. J. Cowles, in *Handbook of Scaling Methods in Aquatic Ecology: Measurements, Analysis, Simulation*, L. Seuront, P. G. Strutton, Eds. (CRC, Boca Raton, FL, 2003), pp. 31–49.
18. A. M. Roberts, F. M. Deacon, *J. Fluid Mech.* **452**, 405 (2002).
19. M. Lebert, D. P. Häder, *Nature* **379**, 590 (1996).
20. M. S. Jones, L. Le Baron, T. J. Pedley, *J. Fluid Mech.* **281**, 137 (1994).
21. N. A. Hill, D. P. Häder, *J. Theor. Biol.* **186**, 503 (1997).
22. T. J. Pedley, N. A. Hill, J. O. Kessler, *J. Fluid Mech.* **195**, 223 (1988).
23. Materials and methods are available as supporting material on *Science* Online.
24. D. A. Birch, W. R. Young, P. J. S. Franks, *Deep-Sea Res. Part I Oceanogr. Res. Pap.* **55**, 277 (2008).
25. D. Kamykowski, R. E. Reed, G. J. Kirkpatrick, *Mar. Biol. (Berlin)* **113**, 319 (1992).
26. J. G. Mitchell, H. Yamazaki, L. Seuront, F. Wolk, H. Li, *J. Mar. Syst.* **69**, 247 (2008).
27. M. T. Stacey, M. A. McManus, J. V. Steinbuck, *Limnol. Oceanogr.* **52**, 1523 (2007).
28. J. O. Kessler, *Prog. Phycol. Res.* **4**, 257 (1986).
29. L. T. Mouritsen, K. Richardson, *J. Plankton Res.* **25**, 783 (2003).
30. R. Stocker, J. R. Seymour, A. Samadani, D. E. Hunt, M. F. Polz, *Proc. Natl. Acad. Sci. U.S.A.* **105**, 4209 (2008).
31. F. Azam, F. Malfatti, *Nat. Rev. Microbiol.* **5**, 782 (2007).

32. We thank P. Franks, W. Young, D. Grünbaum, T. Cowles, R. Bearon, M. Bees, D. Häder, D. Anderson, M. McManus, and L. Karp-Boss for helpful discussions; T. Peacock for the loan of experimental equipment; T. Clay and S. Stransky for developing BacTrack; R. A. Cattolico for providing *H. akashiwo*; and J. Mitchell, E. DeLong, S. Chisholm, M. Polz, H. Nepf, J. Seymour, J. Bragg, B. Kirkup, P. Reis, D. Birch, and S. Sunghwan for comments on the manuscript. W.M.D. acknowledges a National Defense Science and Engineering Graduate Fellowship. J.O.K. acknowledges support from Department of Energy grant W31-109-ENG38. R.S. acknowledges support from NSF (OCE 0526241 and OCE CAREER 0744641), MIT's Earth Systems Initiative, and a Doherty Professorship.

Supporting Online Material

www.sciencemag.org/cgi/content/full/323/5917/1067/DC1
Materials and Methods
References
Movies S1 and S2

17 October 2008; accepted 7 January 2009
10.1126/science.1167334

Cytosolic Viral Sensor RIG-I Is a 5′-Triphosphate–Dependent Translocase on Double-Stranded RNA

Sua Myong,[1]*† Sheng Cui,[2]* Peter V. Cornish,[3,4] Axel Kirchhofer,[2] Michaela U. Gack,[5,6,7] Jae U. Jung,[5,6] Karl-Peter Hopfner,[2]† Taekjip Ha[1,3,4]†

Retinoic acid inducible–gene I (RIG-I) is a cytosolic multidomain protein that detects viral RNA and elicits an antiviral immune response. Two N-terminal caspase activation and recruitment domains (CARDs) transmit the signal, and the regulatory domain prevents signaling in the absence of viral RNA. 5′-triphosphate and double-stranded RNA (dsRNA) are two molecular patterns that enable RIG-I to discriminate pathogenic from self-RNA. However, the function of the DExH box helicase domain that is also required for activity is less clear. Using single-molecule protein-induced fluorescence enhancement, we discovered a robust adenosine 5′-triphosphate–powered dsRNA translocation activity of RIG-I. The CARDs dramatically suppress translocation in the absence of 5′-triphosphate, and the activation by 5′-triphosphate triggers RIG-I to translocate preferentially on dsRNA in cis. This functional integration of two RNA molecular patterns may provide a means to specifically sense and counteract replicating viruses.

Retinoic acid inducible–gene I (RIG-I) is a cytosolic pattern-recognition receptor that senses pathogen-associated molecular patterns (PAMPs) on viral RNA and triggers an antiviral immune response by activating type-I interferons (IFN-α and -β) (*1*). A 5′-triphosphate moiety on viral RNA is a major PAMP detected by RIG-I as a viral signature (*2*, *3*). 5′-triphosphates arise during viral replication and are absent in most cytosolic RNA because of cleavage or capping

modifications (*4*–*6*). Another PAMP for RIG-I is double-stranded RNA (dsRNA), although it is less effective than 5′-triphosphate (*1*, *7*–*13*). It remains unclear, however, whether these distinct patterns trigger RIG-I signaling independently or whether they are integrated by RIG-I to increase specificity for viral RNA. RIG-I consists of two N-terminal tandem CARDs (caspase activation and recruitment domains), a central DExH box RNA helicase/adenosine triphosphatase (ATPase) domain, and a C-terminal regulatory domain (RD). The CARDs are ubiquitinated by tripartite motif-containing 25 (TRIM25) (*14*), and the ubiquitinated CARDs interact with the CARD on mitochondrial anti-viral signaling (MAVS; also called IPS-1, Cardif, or VISA) on the mitochondrial outer membrane to elicit downstream signaling that leads to IFN expression (*15*–*18*). The C-terminal RD inhibits RIG-I signaling in the absence of viral RNA (*8*) and senses the 5′-triphosphate in order to guide RIG-I to bind viral RNA with high specificity (*19*, *20*). Although the role of CARDs and RD has been characterized, the function of the ATPase domain remains elusive (*21*). A single-point mutation (Lys^{270}→Ala^{270}) in the ATPase site rendered RIG-I inactive in antiviral signaling (*1*), even though it retained RNA-binding ability (*22*). Furthermore, the ATPase activity of RIG-I correlates closely with the dsRNA-induced RIG-I signaling (*13*). However, it is unknown why the ATPase activity is required for RIG-I function.

RNA/DNA helicases usually unwind duplex nucleic acids by translocating on one of the product single strands by using adenosine 5′-triphosphate (ATP) hydrolysis, and their ATPase activity is consequently stimulated by single-stranded (ss) nucleic acids. In contrast, the ATPase activity of RIG-I is stimulated by dsRNA (*19*). We therefore examined whether RIG-I uses ATP hydrolysis to translocate on dsRNA. The dsRNA was made by annealing two complementary 25-nucleotide oligomer ssRNAs, one labeled with 3′-biotin and the other with a 3′-fluorescent label, DY547 (Dharmacon, Lafayette, CO). The dsRNA was tethered to a polymer-passivated quartz surface coated with neutravidin (Fig. 1A). The activity of RIG-I was monitored by a method termed protein-induced fluorescence enhancement (PIFE), which we found to be an effective alternative to fluorescence resonance energy transfer (FRET) (*23*, *24*). The method monitors changes in intensity of a single fluorophore that correlates with proximity of the unlabeled protein (more details and comparison of PIFE and FRET data for Rep helicase translocation are given in fig. S1) (*25*). PIFE can be used to study nucleic acids motors without fluorescent modification and even with high dissociation constant, which would prohibit single-molecule analysis of labeled proteins.

We first tested a RIG-I truncation mutant that lacks both of the CARDs, termed RIGh, because its ATPase activity is efficiently stimulated by dsRNA without the need for 5′-triphosphate on RNA (*19*). Binding of RIGh to dsRNA was visualized as an abrupt rise in the fluorescent signal of a single DY547 after the addition of protein (Fig. 1B). Most molecules (>90%) displayed a steady binding for 20 to 30 s, resulting in a strong fluorescence signal (Fig. 1E). The equilibrium-binding constant calculated from single-molecule binding data, which was collected from several hundred molecules, closely matched those determined using fluorescence anisotropy in bulk solution (fig. S2). When ATP was added together with RIGh, we detected a periodic fluorescence fluctuation, which is indicative of a repetitive translocational movement (Fig. 1, C and D; data obtained at 23°C). Translocation here is defined as directed movement of RIG-I along the axis of dsRNA without unwinding it. Under our conditions, RIG-I does not unwind dsRNA (fig. S3).

At 37°C, RIGh-induced fluctuation of the DY547 signal became more rapid (Fig. 2A). The time interval between successive intensity peaks, denoted by Δt, was determined from many molecules of RIGh translocating on 25–base pair (bp) and 40-bp dsRNA, and the resulting histograms show a single narrow peak with a longer average value for the longer dsRNA (2.9 s for 40 bp and 1.1 s for 25 bp) (Fig. 2B). When 100 nM wild-type RIG-I (wtRIG) was added with 1 mM ATP, the fluorescence signal also showed a gradual fluctuation at regular intervals but at a much-reduced frequency as compared with that of RIGh (Fig. 2C). Δt histograms are peaked at longer times for 40-bp as compared with 25-bp dsRNA (32.6 s versus 18.5 s), and their average values are 15 times higher than those of RIGh (Fig. 2D).

To test the role of ATP in the translocation reaction, the average of Δt, t_{avg}, was determined by Gaussian fitting of Δt histograms over a range of ATP concentrations (fig. S4). The inverse of t_{avg} was plotted versus ATP concentration and fitted well to the Michaelis-Menten equation, yielding K_m of 180 μM (Fig. 2G). The length dependence and ATP dependence show that the ATPase activity of RIG-I powers its translocation on the entire length of dsRNA. The contrast between the

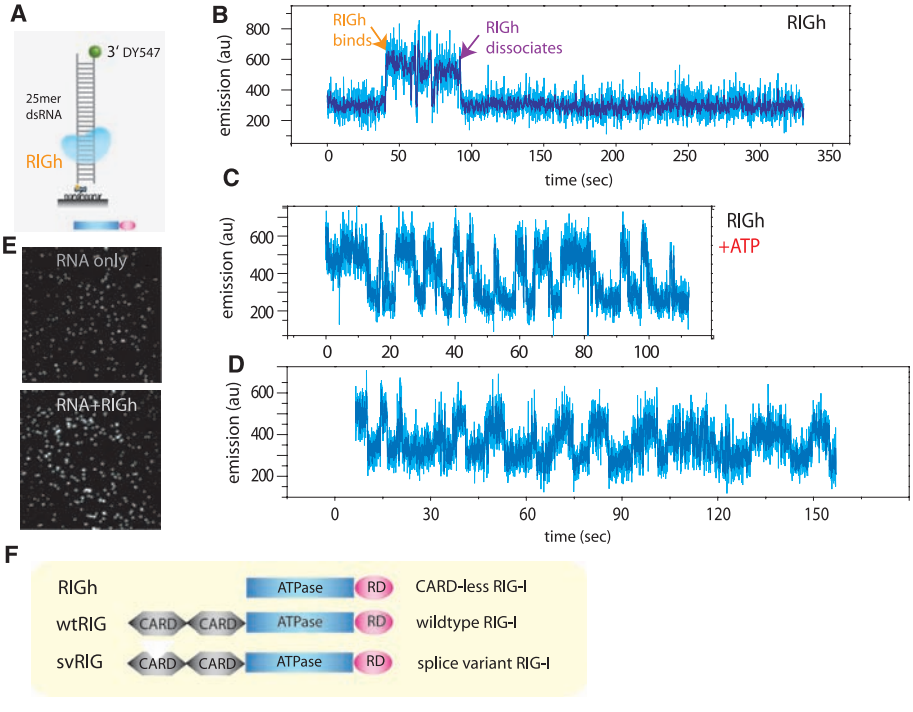

Fig. 1. PIFE visualization of RIG-I binding and translocation. (**A**) dsRNA (25-nucleotide oligomer) with single fluorophore (DY547) was tethered to surface via biotin-neutravidin. (**B**) Addition of RIGh (CARD-less mutant) resulted in an abrupt increase in emission of the fluorophore, indicating RIGh binding because of PIFE. (**C** and **D**) Addition of RIGh with ATP-induced periodic fluctuation of fluorophore. (**E**) The effect of PIFE is visible on the single-molecule imaging surface; fluorescence becomes substantially brighter upon adding RIGh protein. (**F**) Schematic representation of three RIG-I variants used in this study; wtRIG, RIGh, and svRIG are shown.

[1]Institute for Genomic Biology, University of Illinois at Urbana-Champaign, 1206 West Gregory Drive, Champaign, IL 61801, USA. [2]Center for Integrated Protein Science and Munich Center for Advanced Photonics at the Gene Center, Ludwig-Maximilians-University of Munich, Feodor-Lynen-Strasse 25, 81377 Munich, Germany. [3]Department of Physics and Center for the Physics of Living Cells, University of Illinois at Urbana-Champaign, Room 133, Loomis Laboratory, MC 704, 1110 West Green Street, Urbana, IL 61801, USA. [4]Howard Hughes Medical Institute, Urbana, IL, USA. [5]Department of Molecular Microbiology and Immunology, University of Southern California, Keck School of Medicine, Harlyne J. Norris Cancer Research Tower, 1450 Biggy Street, Los Angeles, CA 90033, USA. [6]Department of Microbiology and Molecular Genetics and Tumor Virology Division, New England Primate Research Center, Harvard Medical School, 1 Pine Hill Drive, Southborough, MA 01772, USA. [7]Institute for Clinical and Molecular Virology, Friedrich-Alexander-University Erlangen-Nuremberg, Schlossgarten 4, 91054 Erlangen, Germany.

*These authors contributed equally to this work.
†To whom correspondence should be addressed. E-mail: smyong@uiuc.edu (S.M.); hopfner@lmb.uni-muenchen.de (K.-P.H.); tjha@uiuc.edu (T.H.)

slow movement of wtRIG and the 15-fold accelerated movement of RIGh is consistent with the substantially higher stimulation of ATPase activity by dsRNA that was observed in RIGh than was in wtRIG (*19*) and with the report that CARDs inhibit the ATPase activity of RIG-I (*8*).

To further evaluate the regulatory role of CARDs, we tested the RIG-I splice variant, svRIG, which lacks amino acids 36 to 80 in the first CARD (*26*). svRIG confers dominant negativity in antiviral signaling, implying a loss of signaling function arising from a deficient CARD. The translocation activity of svRIG on dsRNA is highly similar to that of RIGh and is characterized by much more rapid fluctuations as compared with wtRIG (Fig. 2, A and F). svRIG translocation is also ATP-dependent with K_m of 114 μM similar to that of RIGh (fig. S5). Thus, CARD-mediated suppression of translocation activity requires complete CARDs.

Apart from dsRNA, a powerful PAMP for RIG-I is 5′-triphosphate (*2*, *22*). To examine if 5′-triphosphate influences the RNA translocation activity of RIG-I, we prepared 5′-triphosphate RNA (86-nucleotide oligomer) via in vitro transcription and annealed it to a complementary 20-nucleotide oligomer DNA strand. The DNA strand was modified with a 3′ fluorophore (Cy3) and 5′ biotin, which serves as a fluorescence reporter and a surface-tethering point, respectively (Fig. 3A). Addition of wtRIG and ATP to this substrate resulted in extremely rapid fluctuations in the fluorescence signal (Fig. 3, B and C). The rate of translocation, calculated as $(t_{avg})^{-1}$, was dependent on the ATP concentration, with a K_m value of 37 μM (fig. S6). RIGh showed translocation activity on 5′-triphosphate RNA with a rate comparable with wtRIG (Fig. 3, D and E).

wtRIG's translocation on 5′-triphosphate RNA is over 20 times faster than on dsRNA (t_{avg} of 18.5 s versus 0.85 s) (Figs. 1C and 3C). Combined with the data on RIGh and svRIG that showed rapid dsRNA translocation activity regardless of the presence of 5′-triphosphate, we conclude that (i) intact CARDs are necessary to negatively regulate the dsRNA translocation activity of RIG-I and (ii) recognition of 5′-triphosphate by RD completely lifts the suppression by CARDs. Therefore, RNA translocation of RIG-I is regulated by its N-terminal (CARD) and C-terminal (RD) domains. Because the immobilized RNA molecules are more than 1 μm apart from each other, the effect of 5′-triphophate must be in cis; that is, RIG-I translocates rapidly on the same RNA that presents 5′-triphosphate. Adding up to 100 times molar excess of 5′-triphosphate–containing ssRNA strand did not increase the translocation rate of wtRIG on dsRNA (fig. S7).

The 5′-triphosphate RNA we used has both single-stranded and double-stranded portions, and the double-stranded portion is a RNA/DNA heteroduplex. Studies on various nucleic acid substrates showed that RIG-I is an RNA-specific translocase that tracks one RNA strand either on dsRNA or RNA/DNA heteroduplexes (figs. S8 and S9). Does RIG-I, upon recognition of 5′-triphosphate, translocate on the ssRNA, the duplex region, or both? To answer this question, we progressively lengthened the duplex from 20 to 50 bp while progressively shortening the single-stranded region proximal to 5′-triphosphate from 66 to 36 nucleotides (nt) (Fig. 4A). t_{avg} of both wtRIG and RIGh increased linearly with the duplex length, demonstrating translocation on duplex rather than ssRNA (Fig. 4B and fig. S10). Varying the ssRNA tail length while keeping the same length dsRNA did not change t_{avg} (Fig. 4, C and D, and fig. S11). The asymmetric PIFE signal on the heteroduplexes indicates 5′ to 3′ translocation directionality (fig. S12).

The highly periodic repetitive nature of the translocation signal, reminiscent of *Escherichia coli* Rep and Hepatitis C virus NS3 helicases (*27*, *28*), suggests that a single unit of RIG-I repeatedly moves on one RNA without dissociation. This was further verified by washing the reaction chamber with ATP-containing buffer devoid of protein, which left a majority of molecules still in repetitive motion (fig. S13). As a further test, we labeled RIGh nonspecifically with the acceptor fluorophore, and performed single-molecule FRET experiments on the donor-labeled RNA. Periodic anticorrelated changes of the donor and acceptor intensities, consistent with RIG-I translocation on RNA (fig. S14), were observed.

The dsRNA translocation activity on RNA that contains 5′-triphosphate would serve as a signal verification mechanism by activating the ATPase only if the RNA features both PAMPs, the 5′-triphosphate, and dsRNA. Thus, our data not only suggest a functional connection between the apparently different PAMPs but also indicate that integration of more than one PAMP in a single activation mechanism could be important for the selective distinction of host from viral RNA.

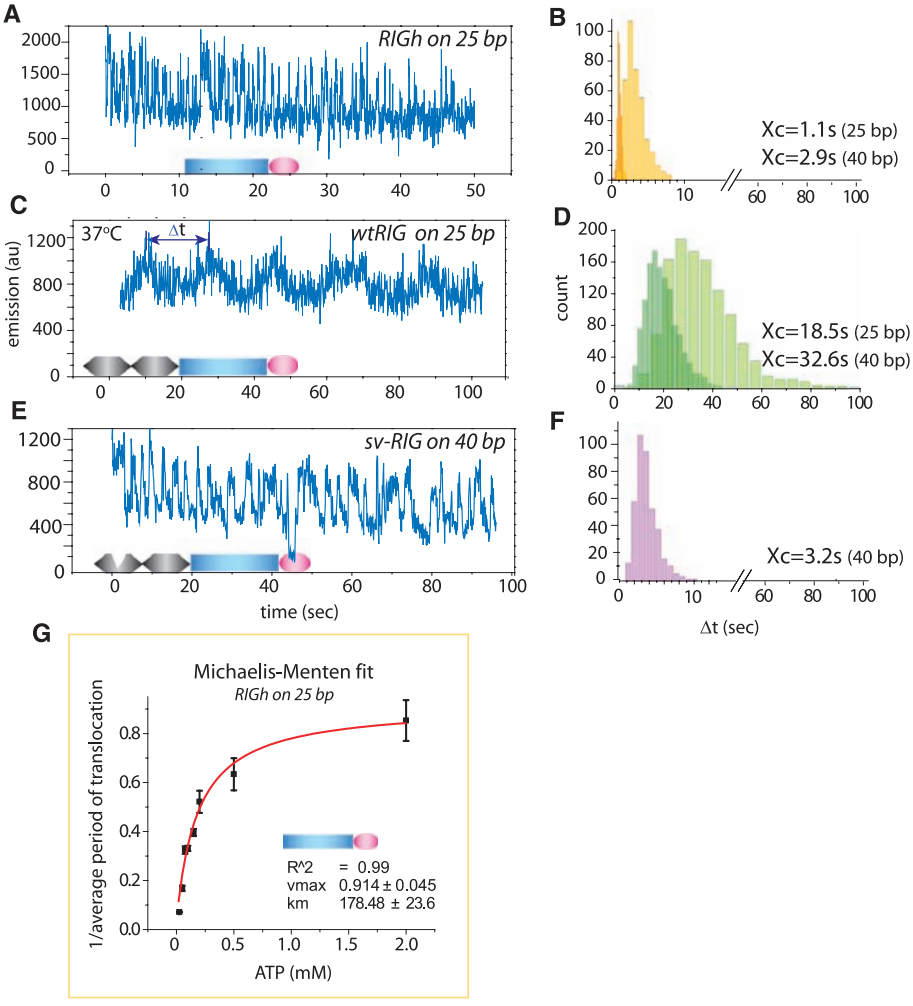

Fig. 2. RIG-I translocates on dsRNA, and CARD is inhibitory. (**A**, **C**, and **E**) 100 nM RIGh, wtRIG, and svRIG were added with 1 mM ATP, respectively, at 37°C. The signal fluctuation represents RIG-I movement along the dsRNA substrate. (**B**, **D**, and **F**) Dwell-time analysis of periods denoted by Δ*t* with a double arrow (C) was measured for many molecules and plotted as histograms for RIGh (B), wtRIG (D), and svRIG (F) for 25-bp and 40-bp dsRNA. (**G**) The inverse of average Δ*t*, $(t_{avg})^{-1}$, was plotted against an axis of ATP concentration and fitted to the Michaelis-Menten equation. The error bars denote SD from three separate experiments each. The maximum velocity (V_{max}) and substrate concentration at half maximal velocity (K_m) values were 0.91 and 179 μM, respectively.

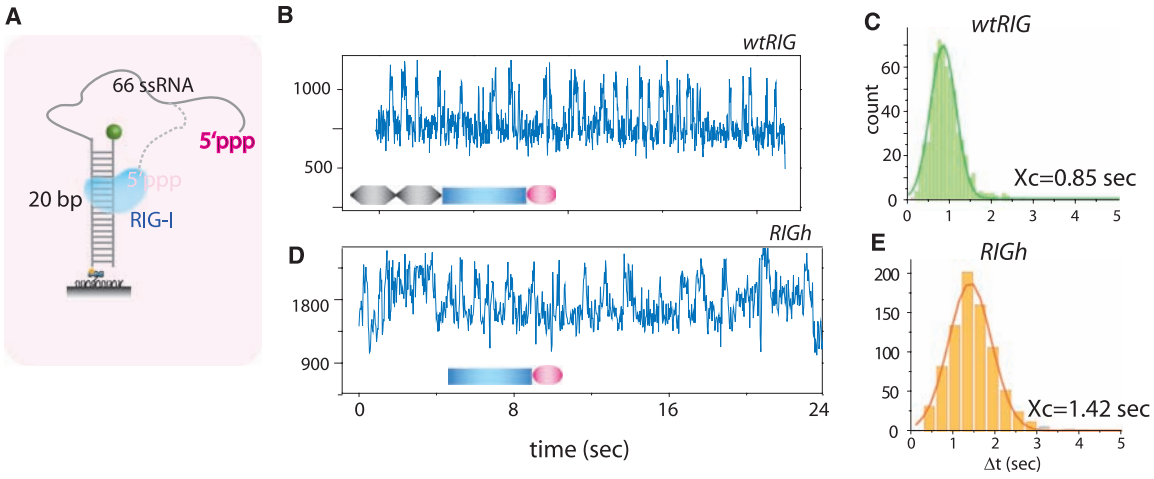

Fig. 3. 5′-triphosphate accelerates RIG-I translocation activity. (**A**) The translocation assay was performed on a 5′-triphosphate–containing substrate that consists of 86-nucleotide oligomer ssRNA from in vitro transcription annealed to complementary 20-nucleotide oligomer ssDNA with 3′ Cy3 and 5′ biotin. (**B** and **D**) Activity of wtRIG was greatly stimulated by the presence of 5′-triphosphate. The data shown were taken at room temperature because of an extremely fast kinetic rate observed at 37°C. RIGh also showed robust translocation activity on this substrate. (**C** and **E**) Dwell-time analysis indicates that wtRIG showed a slightly higher rate of translocation than did RIGh.

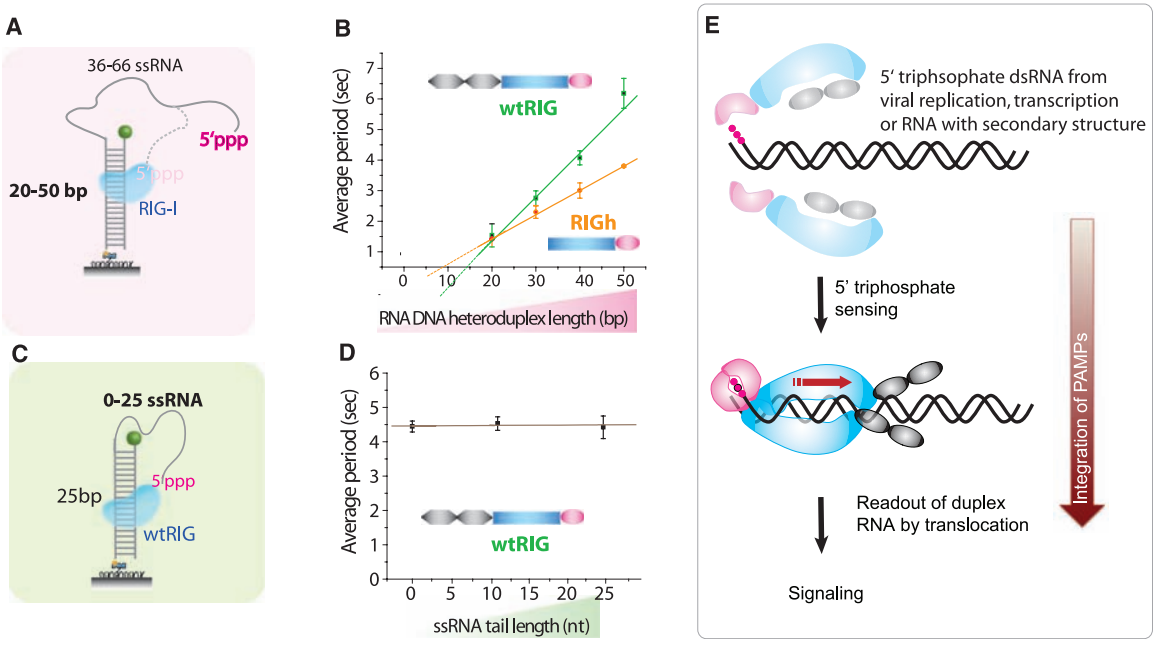

Fig. 4. RIG-I translocates on a double strand of 5′-triphosphate RNA. (**A**) To identify the region of translocation, the double-strand length was varied from 20 to 50 bp, whereas the ssRNA length was varied from 66 to 36 nt, respectively. (**B**) t_{avg} versus duplex length. (**C**) Three constructs were prepared with the fixed dsRNA length of 25 bp and variable ssRNA tail length of 0, 10, and 25 nt. (**D**) t_{avg} versus ssRNA tail length. Error bars denote SD from three separate experiments each. (**E**) Proposed mechanism for PAMP signal integration by RIG-I. Binding of RIG-I regulatory domain (pink) to RNA 5′ triphosphates(for example, arising from virus replication or transcription) dimerizes RIG-I and activates the translocase domain (blue). Further recognition of dsRNA stimulates ATPase activity, resulting in translocation (red arrow), a process that may induce a signaling conformation with exposed CARDs (gray). Precise domain arrangements are speculative and depicted here for illustrative purposes.

What is the molecular function of the translocase activity? Translocation might effectively interfere with viral proteins by preventing them from binding, blocking their progression, or displacing them, thus actively interfering with viral replication (*29*). However, such a function does not explain why an ATPase-deficient mutation of RIG-I lacks signaling activity. Perhaps repetitive shuttling at dsRNA regions of the viral genome, which may arise from genome replication, transcription, or stable secondary structures, could provide a structural conformation in RIG-I with exposed CARDs to attract the next players in the signaling cascade (Fig. 4E). The signal strength is likely related to the amount of time spent in translocation mode and therefore to the length of RNA. This might explain how RIG-I and melanoma differentiation-associated protein-5 (MDA5) may differentially read out very long dsRNA regions (*13*). Finally, our finding of RIG-I as a dsRNA translocase completes the range of activities in superfamily 2 DExH box ATPases, which now include single-strand– and double-strand–specific translocases for both RNA and DNA (*30*).

References and Notes

1. M. Yoneyama *et al.*, *Nat. Immunol.* **5**, 730 (2004).
2. V. Hornung *et al.*, *Science* **314**, 994 (2006).
3. A. Pichlmair *et al.*, *Science* **314**, 997 (2006).
4. A. J. Shatkin, J. L. Manley, *Nat. Struct. Biol.* **7**, 838 (2000).
5. M. Fromont-Racine, B. Senger, C. Saveanu, F. Fasiolo, *Gene* **313**, 17 (2003).
6. R. Singh, R. Reddy, *Proc. Natl. Acad. Sci. U.S.A.* **86**, 8280 (1989).
7. R. Sumpter Jr. *et al.*, *J. Virol.* **79**, 2689 (2005).
8. T. Saito *et al.*, *Proc. Natl. Acad. Sci. U.S.A.* **104**, 582 (2007).
9. J. T. Marques *et al.*, *Nat. Biotechnol.* **24**, 559 (2006).
10. P. Gee *et al.*, *J. Biol. Chem.* **283**, 9488 (2008).
11. C. E. Samuel, *Clin. Microbiol. Rev.* **14**, 778 (2001).
12. H. Kato *et al.*, *Nature* **441**, 101 (2006).
13. H. Kato *et al.*, *J. Exp. Med.* **205**, 1601 (2008).
14. M. U. Gack *et al.*, *Nature* **446**, 916 (2007).
15. E. Meylan *et al.*, *Nature* **437**, 1167 (2005).
16. R. B. Seth, L. Sun, C. K. Ea, Z. J. Chen, *Cell* **122**, 669 (2005).
17. L. G. Xu *et al.*, *Mol. Cell* **19**, 727 (2005).
18. T. Kawai *et al.*, *Nat. Immunol.* **6**, 981 (2005).
19. S. Cui *et al.*, *Mol. Cell* **29**, 169 (2008).
20. K. Takahasi *et al.*, *Mol. Cell* **29**, 428 (2008).

21. M. Yoneyama, T. Fujita, *Immunity* **29**, 178 (2008).
22. S. Plumet *et al.*, *PLoS One* **2**, e279 (2007).
23. G. Luo, M. Wang, W. H. Konigsberg, X. S. Xie, *Proc. Natl. Acad. Sci. U.S.A.* **104**, 12610 (2007).
24. C. J. Fischer, N. K. Maluf, T. M. Lohman, *J. Mol. Biol.* **344**, 1287 (2004).
25. Materials and methods are available as supporting material on *Science* Online.
26. M. U. Gack *et al.*, *Proc. Natl. Acad. Sci. U.S.A.* **105**, 16743 (2008).
27. S. Myong, I. Rasnik, C. Joo, T. M. Lohman, T. Ha, *Nature* **437**, 1321 (2005).
28. S. Myong, M. M. Bruno, A. M. Pyle, T. Ha, *Science* **317**, 513 (2007).
29. E. Jankowsky, C. H. Gross, S. Shuman, A. M. Pyle, *Science* **291**, 121 (2001).
30. H. Durr, C. Korner, M. Muller, V. Hickmann, K. P. Hopfner, *Cell* **121**, 363 (2005).
31. We thank C. Joo and K. Ragunathan for careful review of the manuscript. This work was supported by NIH grant R01-GM065367 and NSF Physics Frontiers Center grant 0822613 to T.H., NIH grant CA82057 to J.U.J., and a Human Frontiers of Science grant to T.H. and K.-P.H. K.-P.H. acknowledges support from the German Excellence Initiative. S.C. is supported by Deutsche Forschungsgemeinschaft (DFG) program project 455 to K.-P.H. A.K. acknowledges support from the DFG graduate school 1202. T.H. is an investigator with the Howard Hughes Medical Institute. S.M. is a fellow at the Institute for Genomic Biology.

Supporting Online Material
www.sciencemag.org/cgi/content/full/1168352/DC1
Materials and Methods
Figs. S1 to S14
References

11 November 2008; accepted 15 December 2008
Published online 1 January 2009;
10.1126/science.1168352
Include this information when citing this paper.

Neuronal Activity–Induced Gadd45b Promotes Epigenetic DNA Demethylation and Adult Neurogenesis

Dengke K. Ma,[1,2*†] Mi-Hyeon Jang,[1,3*] Junjie U. Guo,[1,2] Yasuji Kitabatake,[1,3] Min-lin Chang,[1,3] Nattapol Pow-anpongkul,[1] Richard A. Flavell,[4] Binfeng Lu,[5] Guo-li Ming,[1,2,3] Hongjun Song[1,2,3†]

The mammalian brain exhibits diverse types of neural plasticity, including activity-dependent neurogenesis in the adult hippocampus. How transient activation of mature neurons leads to long-lasting modulation of adult neurogenesis is unknown. Here we identify *Gadd45b* as a neural activity–induced immediate early gene in mature hippocampal neurons. Mice with *Gadd45b* deletion exhibit specific deficits in neural activity–induced proliferation of neural progenitors and dendritic growth of newborn neurons in the adult hippocampus. Mechanistically, *Gadd45b* is required for activity-induced DNA demethylation of specific promoters and expression of corresponding genes critical for adult neurogenesis, including brain-derived neurotrophic factor and fibroblast growth factor. Thus, Gadd45b links neuronal circuit activity to epigenetic DNA modification and expression of secreted factors in mature neurons for extrinsic modulation of neurogenesis in the adult brain.

Adult neurogenesis represents a prominent form of structural plasticity through continuous generation of new neurons in the mature mammalian brain (*1*, *2*). Similar to other neural activity-induced plasticity with fine structural changes within individual neurons, adult neurogenesis is modulated by a plethora of external stimuli (*1*, *2*). For example, synchronized activation of mature dentate neurons by electroconvulsive treatment (ECT) in adult mice causes sustained up-regulation of hippocampal neurogenesis (*3*) without any detectable cell damage (fig. S1). How transient activation of mature neuronal circuits modulates adult neurogenesis over days and weeks is largely unknown.

Epigenetic mechanisms potentially provide a basis for such long-lasting modulation (*4*). We examined the expression profiles of known epigenetic regulators in response to ECT, including those involved in chromatin modification (*5*). One gene that we found to be strongly induced by ECT was *Gadd45b* (Fig. 1A) (*6*), a member of the *Gadd45* family previously implicated in DNA repair, adaptive immune response (*7*–*10*), and DNA 5-methylcytosine excision in cultured cells (*11*). We first characterized *Gadd45b* induction by neuronal activity in the adult hippocampus (*5*). Analysis of microdissected dentate gyrus tissue showed robust, transient induction of *Gadd45b* expression by a single ECT (Fig. 1A, fig. S2, and table S1). In situ analysis revealed induction largely in $NeuN^+$ mature dentate granule cells (Fig. 1B and fig. S3). Spatial exploration of a novel environment, a behavioral paradigm that activates immediate early genes (IEGs) (*12*), also led to significant induction of *Gadd45b*, but not *Gadd45a* or *Gadd45g* (Fig. 1, C and D). Most Gadd45b-positive cells also expressed Arc (Fig. 1D) (88 ± 3%, $n = 4$), a classic activity-induced IEG. Thus, physiological stimulation is sufficient to induce *Gadd45b* expression in dentate granule cells. Experiments with pharmacological manipulations of primary hippocampal neurons further suggested that *Gadd45b* induction by activity requires the *N*-methyl-D-aspartate receptor (NMDAR), Ca^{2+}, and calcium/calmodulin-dependent protein kinase signaling (fig. S4 and supporting text). In vivo injection of the NMDAR antagonist +3-(2-carboxypiperazin-4-yl)-propyl-1-phosphonic acid (CPP) abolished ECT-induced *Gadd45b* and *Arc* expression in the adult dentate gryus (Fig. 1E). Together, these results suggest that *Gadd45b* shares the same induction pathway as classic activity-induced IEGs (*13*).

We next assessed whether *Gadd45b* induction is required for neural activity–dependent adult neurogenesis. Adult *Gadd45b* knockout (KO) (*10*) mice appeared anatomically normal (fig. S5) and exhibited identical NMDAR-dependent induction of known IEGs at 1 hour after ECT (Fig. 1E). To examine neural progenitor proliferation, adult mice at 3 days after ECT or sham treatment were injected with bromodeoxyuridine (BrdU) and killed 2 hours later (*5*). Stereological counting showed similar densities of $BrdU^+$ cells in the dentate gyrus between wild-type (WT) and KO mice without ECT (Fig. 2). After ECT, however, there was a 140% increase in the density of $BrdU^+$ cells in WT mice and only a 40% increase in KO littermates (Fig. 2). Little caspase-3 activation was detected within the dentate gyrus under all these conditions (figs. S1 and S6), ruling out a potential contribution from cell death. To confirm this finding with a manipulation of better spatiotemporal control, we developed effective lentiviruses to reduce the expression of endogenous *Gadd45b* with short-hairpin RNA (shRNA) (fig. S7). Expression of shRNA-*Gadd45b* through stereotaxic viral injection largely abolished ECT-induced proliferation of adult neural progenitors, whereas the basal proliferation was similar to that of shRNA-control (fig. S7). We also examined exercise-induced adult neurogenesis, a physiological stimulation that induced a modest increase in *Gadd45b* expression (fig. S8A). A 7-day running program led to a marked increase of neural progenitor proliferation in adult WT mice, but was significantly less effective in their KO littermates (fig. S8B). Together, these results demonstrate a specific and essential role of *Gadd45b* in activity-induced, but not basal, proliferation of neural progenitors in the adult dentate gyrus.

We next examined the role of *Gadd45b* induction in the dendritic development of newborn

[1]Institute for Cell Engineering, Johns Hopkins University School of Medicine, 733 North Broadway, Baltimore, MD 21205, USA. [2]The Solomon H. Snyder Department of Neuroscience, Johns Hopkins University School of Medicine, 733 North Broadway, Baltimore, MD 21205, USA. [3]Department of Neurology, Johns Hopkins University School of Medicine, 733 North Broadway, Baltimore, MD 21205, USA. [4]Department of Immunobiology, Howard Hughes Medical Institute, Yale University School of Medicine, 300 Cedar Street, New Haven, CT 06520, USA. [5]Department of Immunology, University of Pittsburgh, School of Medicine, Pittsburgh, PA 15261, USA.

*These authors contributed equally to this work.
†To whom correspondence should be addressed. E-mail: shongju1@jhmi.edu (H.S.); dma2@jhmi.edu (D.K.M.)